


Sensitive pathogen DNA detection by a multi-guide RNA Cas12a assay favoring trans- versus cis-cleavage

Received: 18 February 2025

Accepted: 11 August 2025

Published online: 17 September 2025

 Check for updates

Zhen Huang^{1,2,3,4}✉, Zhe Song³, Jianfeng Zeng³, Xuhui Liu⁵, Mutong Fang³, Zhiyuan Wu⁶, Yao Zhao³, Yanli Chen⁶, Dan Li³, Huan Huang^{1,5}, Liang Fu³, Peng Xu³, Bo Ning^{1,2}, Jun Chen⁷, Ming Guan^{1,2}, Lin Sun⁸, Christopher J. Lyon^{1,2}, Xiao-Yong Fan^{1,2}, Shuihua Lu³✉ & Tony Hu^{1,2}✉

Most CRISPR assays lack clinical utility due to their complex workflows and limited validation. Here we present a streamlined “one-pot” asymmetric CRISPR tuberculosis assay that attenuates amplicon degradation to achieve 5 copies/μL sensitivity within 60 min and detect positive patient samples within 15 min. This assay exhibited 93%, 83%, and 93% sensitivity with adult respiratory, pediatric stool, and adult cerebral spinal fluid specimens, and detected 64% of clinically diagnosed tuberculous meningitis cases, in a cohort of 603 clinical samples. This assay achieves complete specificity and greater sensitivity (74% vs. 56%) than the most sensitive reference test with prospectively collected tongue swabs, and exhibits similar performance when adapted to a lateral flow assay format and employed to analyze self-collected tongue swabs. These results demonstrate the utility of this approach across diverse specimen types, including those suitable for use in remote and resource-limited settings, to improve access to molecular diagnostics.

Molecular diagnostic advances have substantially improved disease diagnosis, as revealed during the COVID-19 pandemic, and can facilitate early intervention and personalized treatment^{1,2}. However, half the global population has limited access to such tests¹, obscuring the true burden of many diseases, particularly those linked to poverty^{3,4}, and increasing their mortality and socio-economic consequences¹. For example, *Mycobacterium tuberculosis* (*Mtb*) infections are responsible for an estimated 10 million new tuberculosis (TB) cases and 1.6 million TB-related deaths annually³, which disproportionately affect low- and middle-income countries⁵ where >35% of new cases go undiagnosed^{1,3}. There is thus an urgent need to develop streamlined diagnostics that

address diagnostic challenges faced by poor, rural, and marginalized communities.

CRISPR-based assays provide a means to rapidly detect specific pathogen-derived nucleic acid sequences for disease diagnosis, and employ ribonucleoprotein (RNP) complexes composed of a CRISPR-associated (Cas) protein and a guide RNA (gRNA) to bind a target sequence and cleave a ssDNA reporter, but have issues that limit their clinical translation^{6–8}. For example, amplification-free CRISPR assays have shown promise for COVID-19 testing^{9,10}, but usually require relatively high concentrations of pathogen-derived nucleic acid for effective diagnosis, whereas *Mtb* DNA concentrations are low in most

¹Center for Cellular and Molecular Diagnostics, Tulane University School of Medicine, New Orleans, LA, USA. ²Department of Biochemistry and Molecular Biology, Tulane University School of Medicine, New Orleans, LA, USA. ³National Clinical Research Center for Infectious Diseases, Shenzhen Third People's Hospital, Southern University of Science and Technology, Shenzhen, Guangdong, China. ⁴Department of Medicine, Tulane School of Medicine, New Orleans, LA, USA. ⁵Department of Tuberculosis, Shanghai Public Health Clinical Center, Fudan University, Shanghai, China. ⁶Department of Laboratory Medicine, Huashan Hospital, Fudan University, Shanghai, China. ⁷Department of Infectious Diseases and Immunology, Shanghai Public Health Clinical Center, Fudan University, Shanghai, China. ⁸Beijing Children's Hospital, Capital Medical University, National Clinical Research Center for Respiratory Diseases, National Center for Children's Health, Beijing, China. ✉e-mail: zhenhuang@tulane.edu; lushuihua66@126.com; tonyhu@tulane.edu

diagnostic specimens^{11,12}. Some studies have employed multiple gRNA to enhance reporter cleavage and signal production but these assays have yielded only moderate sensitivity increases^{9,12,13}. Most CRISPR-based TB diagnostics therefore employ a two-step process that pre-amplifies the target to increase signal production^{6,10}. This approach has been adapted for TB diagnosis, and can detect trace *Mtb* DNA levels in aseptic body fluids to enable TB diagnosis in populations that have difficulty producing diagnostic sputum specimens^{11,12,14}. However, clinical adoption of such tests has been delayed by their lack of clinical validation studies; complex workflows that are impractical for use in clinical applications, especially in resource-limited settings; and significant contamination risks¹⁰.

Streamlined “one-pot” assays that integrate target amplification and detection reactions in a single tube can avoid these issues but be difficult to develop, particularly for low-abundance pathogens, as such assays must be optimized for reaction condition differences and balance amplicon production and cleavage to optimize their sensitivity^{10,15–17}. Some groups developing one-pot assays have employed target sequences with adjacent non-consensus protospacer-adjacent motifs (PAMs) to attenuate cleavage activity^{16,17} since this motif facilitates dsDNA unwinding in Cas12a RNPs^{8,18}, while others have employed gRNA modifications to reduce both RNP affinity and cleavage activity¹⁹. However, while both approaches can attenuate Cas12a cis-cleavage activity to increase target accumulation, they can also attenuate trans-cleavage of the assay reporter to reduce sensitivity.

Here we hypothesized that we could enhance the sensitivity of isothermal one-pot recombinase polymerase amplification (RPA)-CRISPR assays by using gRNAs that favor Cas12a *trans*- vs. *cis*-cleavage activity, as this should favor target accumulation that drives reporter trans-cleavage, and that sensitivity could be further enhanced by the use of Cas12a RNPs targeting distinct sites on their target amplicon. We therefore developed a one-pot asymmetric cis/trans CRISPR cleavage assay for TB (ActCRISPR-TB) that employed multiple gRNAs favoring *trans*- vs. *cis*-cleavage activity upon recognition of their targets within an *Mtb*-specific insertion sequence. In an analysis of 603 clinical specimens from 479 individuals, ActCRISPR-TB diagnostic performance was comparable to reference molecular diagnostics when analyzing respiratory samples, but was greater than these tests when applied to non-respiratory specimens, and markedly enhanced *Mtb* DNA detection in tongue swabs. No loss in analytical or diagnostic sensitivity was observed when this assay was adapted to a lateral flow assay (LFA) format that analyzed self-collected tongue swab specimens suitable for use in streamlined active TB disease finding and screening efforts.

Results

ActCRISPR-TB development and characterization

We have previously described a two-step CRISPR-based TB assay that detects cell-free *Mtb* DNA in serum/plasma of TB patients using a gRNA (gRNA-0, Table S1) that recognizes a site in the multi-copy *Mtb* complex-specific IS6110 insertion element with a canonical PAM (TTTV)¹¹. However, an integrated one-pot assay derived from this assay exhibited delayed and attenuated signal, likely due to a competitive cis-cleavage of the RPA amplicon by its Cas12a RNP (Fig. S1)^{16,17}. Since gRNAs targeting sequences that lack canonical PAM sites (non-canonical gRNAs) can yield differential cis-cleavage vs. trans-cleavage activity, we tiled the IS6110 amplicon sequence to identify non-canonical gRNA candidates that had stable secondary structures (Fig. 1a and S2–S3; Table S1). All gRNAs had strong target specificity but variable cis- and trans-cleavage activities as determined by monitoring the activity of the RNPs to deplete their dsDNA substrate and ssDNA reporter (Fig. 1b–d, S4–S6; Table S2–S3)^{16,20}. All non-canonical gRNAs produced weaker cis-cleavage activity than gRNA-0, although trans-cleavage activities detected with gRNA-2, -5, and -0 were comparable, and substantially greater than the those of the other five gRNAs (12–42% of gRNA-0 activity) (Fig. 1d).

These results agreed with reports that the cis- and trans-cleavage activities of Cas12a are functionally independent^{21,22}, while reanalysis of publicly available datasets from a recent study identified another non-canonical gRNA yielding asymmetric Cas12a cleavage activity (Fig. S7)²³. Structural modeling of the Cas12a RNPs employed in our study detected similar Cas12a and gRNA-template heteroduplex structures but divergence in the relative positions of the non-template strands in proximity to Cas12a catalytic site (Fig. S8), which could potentially influence their asymmetric cleavage activity.

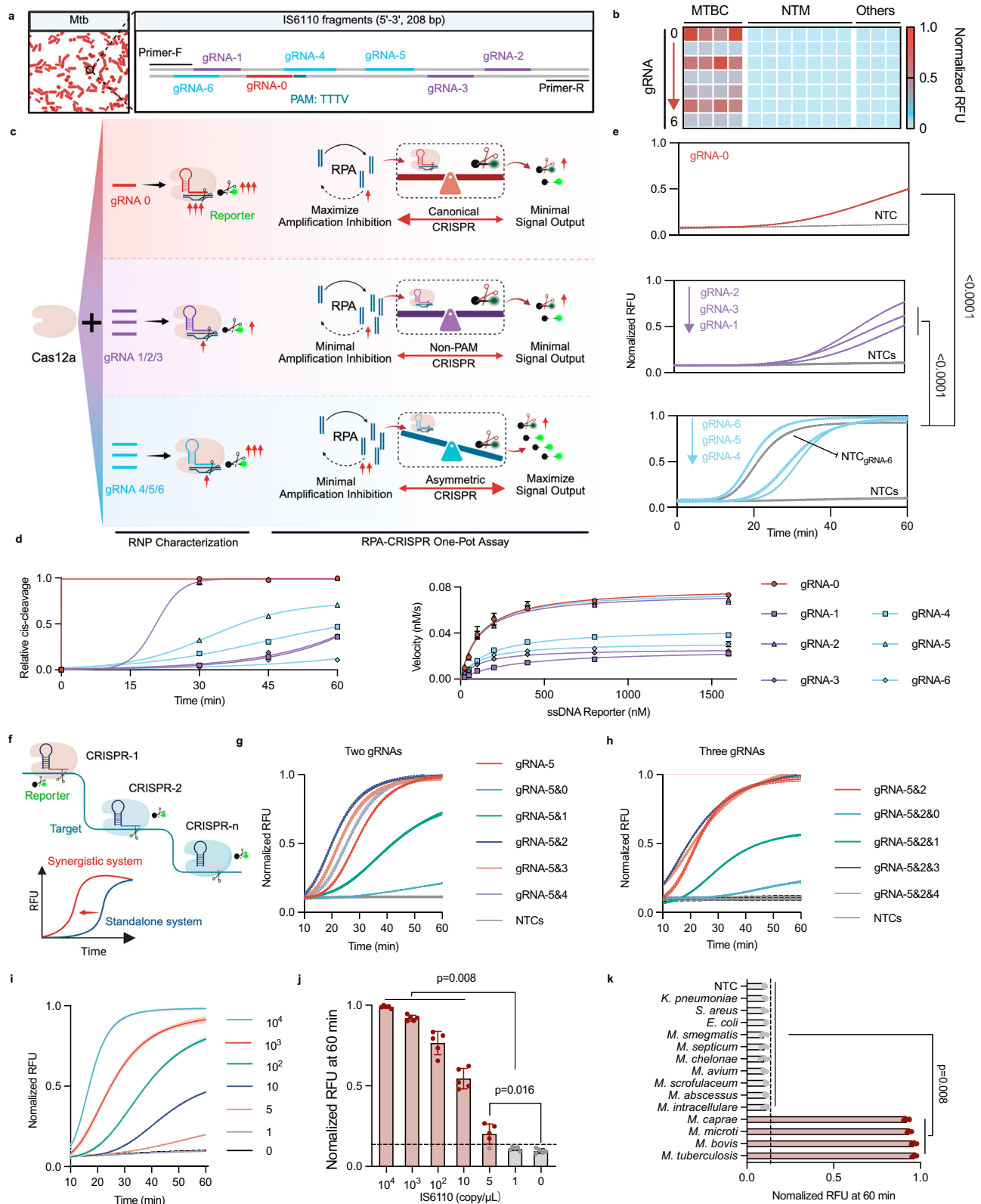
Normalized activity comparisons (Table S4) revealed that gRNA-4, gRNA-5, and gRNA-6 differentially promoted trans- vs. cis-cleavage, and one-pot assays performed with these three gRNAs revealed better reaction kinetics than the four gRNAs that had more balanced cis- and trans-cleavage activities (Fig. 1e), suggesting asymmetric activity reduced amplicon cleavage to improve amplification efficiency, Cas12a trans-cleavage kinetics, and assay signal (Fig. 1c). However, assay signal generated by gRNA-6 was template independent and apparently derived from a 10-nucleotide sequence overlap with the RPA forward primer (Fig. 1a, S2 and S10). This gRNA was thus excluded from all subsequent analyses.

Since gRNA-5 revealed the best reaction kinetics, the RPA and CRISPR reaction conditions of the gRNA-5-based one-pot ActCRISPR-TB assay were optimized to maximize signal (Fig. S11) and minimize the half-maximum signal time (Fig. S12). Subsequent analyses were performed using these conditions (500 nM primers, 16.8 nM Mg²⁺, and 40 nM RNP), as alternate parameters yielded less favorable kinetics. Primer increases tended to reduce RPA efficiency, Mg²⁺ increases reduced assay signal, and reporter increases had no prominent effect on assay kinetics so that a 600 nM concentration was selected to minimize background and assay expense. Comparable ActCRISPR-TB end results were obtained across a 36–40 °C temperature range and with RPA reagents from different manufacturers.

We hypothesized that assays employing distinct Cas12a RNPs could increase signal (Fig. 1f), as previously reported for an amplification-free CRISPR system¹¹, and found that adding other gRNAs to an optimized ActCRISPR-TB gRNA-5 assay with a constant total gRNA concentration differentially increased (gRNA-2 > gRNA-3 > gRNA-4) or decreased (gRNA-0 >> gRNA-1) its kinetics (Fig. 1g). Signal increases induced by gRNA additions were influenced by the relative gRNA ratios: slightly shifting the gRNA-5 to gRNA-2 ratio to favor gRNA-5 (30:10) modestly enhanced signal, whereas a corresponding decrease (10:30) markedly attenuated assay kinetics and signal (Fig. S13), likely due to the greater cis-cleavage activity associated with gRNA-2. Adding gRNA-3 or gRNA-4 to a gRNA-2/gRNA-5 assay modestly increased its kinetics, while adding gRNA-1 or gRNA-0 had the opposite effect (Fig. 1h and S14). Multi-gRNA ActCRISPR-TB assays that used gRNA-2, -3, and -5 achieved a limit of detection (LoD) of 5 copies/μL (Fig. 1i, j)—20 times lower than a one-pot assay using canonical gRNA-0 (Fig. S15)—while retaining specificity for *Mtb* complex species (Fig. 1k).

ActCRISPR-TB diagnostic performance with pulmonary and extrapulmonary specimens

This ActCRISPR-TB assay was next systematically evaluated for its diagnostic performance when used to analyze different types of cryopreserved specimens (Figs. 2a and 3a). Sputum samples with high to very low Xpert grades, as assigned by their Ct values, were DNA-extracted and analyzed to determine the minimum time required for sensitive detection of positive samples (Fig. 3b). Most Xpert-positive sputum DNA isolates (85%; 17 of 20) revealed at least weak ActCRISPR-TB signal by 15 min, with false-negative results detected only in samples with low or very low Xpert grades. Maximum diagnostic sensitivity (95%; 19 of 20 samples) was achieved by 45 min, and the remaining false-negatives did not differ from Xpert-negative specimens at



60-min. A 45-min read time was thus selected to optimize assay time and performance. A subsequent ActCRISPR-TB validation study performed with 56 Xpert-positive and 56 Xpert-negative sputum specimens from adults with presumed TB (Table S5) yielded comparable performance, misclassifying only four samples with low or very low Xpert grades (Fig. 3c and S16) to achieve 93% (95% CI: 83–98%) sensitivity and 100% (95% CI: 94–100%) specificity.

We next evaluated ActCRISPR-TB performance using sputum samples obtained from a cohort of 28 HIV-positive adults with low CD4 counts (median 72 cells/mL; IQR 13.5–158.5) and with and without evidence of TB, since it is frequently more difficult to diagnose TB in this patient population due to the paucibacillary nature of their sputum specimens¹¹. These individuals were post-hoc classified as confirmed, unconfirmed, unlikely, or non-TB cases based on their clinical,

Fig. 1 | Development and characterization of the asymmetric cis/trans-cleavage one-pot CRISPR-TB (ActCRISPR-TB) assay. **a** Schematic of *Mtb* genome IS6110 sites and binding sites for gRNA-0 and six PAM-deficient gRNAs (gRNA-1 to gRNA-6) (Table S1 and Fig. S2). Created in BioRender. Huang, Z. (2025) <https://BioRender.com/a99265m>. **b** Relative specificity of the indicated Cas12a/gRNA RNPs for genomic DNA from four *Mtb* complex (MTBC), seven non-tuberculous mycobacteria (NTM), and three non-mycobacterial species. **c** Dynamic interplay models of RPA and CRISPR reactions in one-pot RPA-CRISPR assays, established using Cas12a/gRNA RNPs with distinct cis- and trans-cleavage activity profiles. Created in BioRender. Huang, Z. (2025) <https://BioRender.com/a99265m>. **d** The cis-cleavage activity (left) and Michaelis–Menten trans-cleavage kinetics (right) of these RNPs, as derived from three experimental and technical replicates, respectively. **e** Signal kinetics of these one-pot RPA/CRISPR assays detected with a positive control (PC;

1000 copies IS6110 DNA/ μ L) and a non-templated control (NTC; nuclease-free water). **f** Schematic depicting the effect of multiple Cas12a/gRNA RNPs to further increase reporter cleavage kinetics. Created in BioRender. Huang, Z. (2025) <https://BioRender.com/wtcfat>. **g, h** CRISPR kinetics detected with **(g)** gRNA-5 or gRNA-5 and gRNA-0, -1, -2, or -4 (1:1 ratio) at constant RNP concentration, or **h** gRNA-5+gRNA-2, with or without gRNA-0, -1, -3, or -4 (6:1 or 3:1 ratio, respectively). One-pot ActCRISPR-TB **i** kinetics and signal detected with the indicated **j** IS6110 DNA concentrations and **k** pathogen genomic DNAs. Data indicate four-parameter logistic (**d**-left, **e, g–i**) and Michaelis–Menten (**d**, right) curve values with 95% confidence intervals (error bars or shaded areas) for representative data, and mean \pm standard deviation (SD) values of five technical replicates of the indicated samples (**j, k**). *P* values were calculated using a two-sided Wilcoxon signed-rank (**e**) and Mann–Whitney tests (**j, k**). Source data are provided as a Source Data file.

laboratory, and treatment data (Table S6). ActCRISPR-TB results demonstrated 80% (95% CI: 44–97%) sensitivity for the confirmed and unconfirmed TB cases, and 89% (95% CI: 65–99%) specificity with unlikely and non-TB cases (Fig. 3d), whereas Xpert MTB/RIF results had 40% sensitivity overall as it detected none of the unconfirmed TB cases. Notably, these results may underestimate ActCRISPR-TB specificity, since the two unlikely TB cases with false-positive results were both culture positive but judged to have non-tuberculous mycobacterial (NTM) infections based on additional findings. However, given the species specificity of the assay, the observation that the remaining four unlikely TB cases with NTM diagnoses all had negative ActCRISPR-TB negative results, and the elevated TB risk in this severely immunocompromised patient cohort, we cannot exclude the possibility that these two unlikely TB patients had both NTM infections and TB.

ActCRISPR-TB performance was next assessed using non-sputum samples, since 25% of symptomatic and >90% of asymptomatic TB cases cannot spontaneously produce sputum²⁴. Lower respiratory tract specimens, including bronchoalveolar lavage fluid (BALF), are often collected to improve diagnosis of such patients²⁵. BALF specimens analyzed in this study were obtained from 47 bacteriologically confirmed TB cases, 19 clinically diagnosed TB cases, and 19 non-TB cases (Fig. 2a; Table S7). Most non-TB cases (66%; 56 of 85) had clinical features of TB but were not diagnosed with TB due to negative sputum test outcomes or missing sputum specimens (Fig. S16). BALF ActCRISPR-TB results identified 96% (45 of 47) of the bacteriologically confirmed TB cases, 21% (4 of 19) of the clinically diagnosed TB cases, and all (19 of 19) non-TB cases (Fig. 3e). Notably, there was a strong correlation between Xpert grade and ActCRISPR-TB signal and positivity for both sputum and BALF specimens (Fig. S17). BALF ActCRISPR-TB results yielded false-negatives for two individuals with “very low” positive Xpert sputum results and identified eight TB cases with false-negative BALF Xpert results (four with microbiologic confirmation and four with clinical diagnosed TB). Overall, ActCRISPR-TB showed high concordance (93%; 95% CI, 89–96%) with Xpert in respiratory specimens, with a pooled sensitivity of 94% (95% CI, 88–98%) and specificity of 92% (95% CI, 85–96%) (Fig. 3f).

ActCRISPR-TB performance was next assessed using stool specimens from a cohort of children with suspected TB, since children are often unable to expectorate sputum and invasive sampling is often not feasible¹¹, leading the WHO to recommend testing stool specimens²⁶. We analyzed archived stool samples from 47 children with presumed TB (Table S8). Only 15 of these children had sputum samples, and just five had positive Xpert Ultra sputum results. However, Xpert Ultra detected *Mtb* DNA in 23 gastric aspirate and 24 stool specimens, whereas ActCRISPR-TB detected 26 positive stool samples, yielding 83% (95% CI: 65–94%) sensitivity and 94% (95% CI: 71–100%) specificity (Figs. 3g and S18).

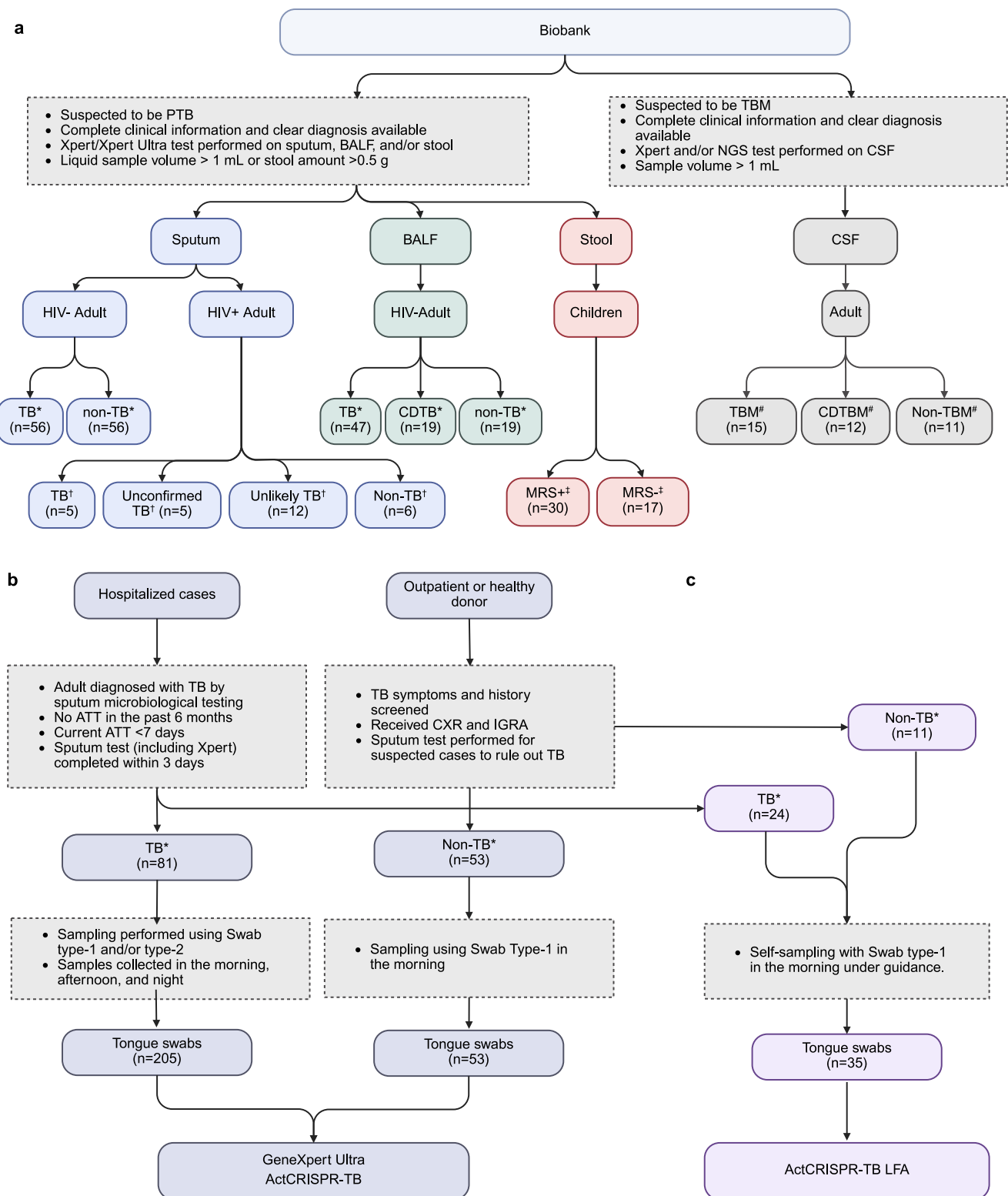
Finally, ActCRISPR-TB was evaluated for its ability to diagnose extrapulmonary tuberculosis (EPTB) since *Mtb* dissemination increases the risk of poor outcomes and death, but direct EPTB diagnosis

requires the analysis of paucibacillary samples obtained from suspected infection sites²⁷. Since tuberculous TB meningitis (TBM) cases require prompt diagnosis and treatment to avoid poor outcomes²⁷, we analyzed cerebrospinal fluid (CSF) specimens from a small cohort of adults with suspected TBM (Fig. 2a; Table S9). ActCRISPR-TB detected 93% (14 of 15) of microbiologically confirmed and 64% (7 of 11) of clinically diagnosed TBM cases (Fig. 3h), yielding 81% overall sensitivity vs. the 35% (9 of 26) overall sensitivity of Xpert. Specificity was not estimated with the non-TBM group since several individuals had pulmonary TB diagnoses and missing CSF clinical test results, which could have yielded false-negative TBM diagnoses. Notably, three of the four non-TBM patients with strong ActCRISPR-TB false-positives had pulmonary TB, and their positives could have reflected *Mtb*-DNA dissemination into the CSF from the circulation (valid false-positives) or early-stage of TBM undetected by other methods (missed true-positives).

ActCRISPR-TB performance with tongue swab specimens

New TB diagnostics that rapidly and accurately analyze accessible specimen types are required to improve access to TB testing and achieve the End TB program’s goal^{2,4,28}. Tongue swabs can simplify specimen collection for pulmonary TB diagnosis since *Mtb* bacilli expelled from the lungs accumulate on the tongue to provide direct evidence of TB disease²⁵. However, sensitive and streamlined assays that can detect trace *Mtb* DNA concentrations in these specimens are required for large-scale active TB screening efforts. We therefore compared ActCRISPR-TB and GeneXpert MTB/RIF Ultra (Xpert Ultra) performance with 205 tongue swab specimens obtained from 134 individuals with microbiologically confirmed TB or non-TB diagnoses, with further analyses performed to examine the effect of swab type and storage conditions (Figs. 2b and 4a, and Table S10). Positive ActCRISPR-TB and Xpert Ultra results were detected for 60 and 45 of these TB cases [74% (95% CI: 63–83%) vs. 56% (95% CI, 44–67%) sensitivity], but not for specimens of the 53 non-TB cases (100% specificity; 95% CI, 93–100%) (Fig. 4b and S19).

ActCRISPR-TB signal intensities for tongue swabs from TB cases with negative and positive sputum culture results markedly differed [median (IQR) values of 509 (447, 1802) vs. 2119 (503, 2119)], and had positive signal frequencies of 38% and 66%, respectively (Fig. 4c). Swab ActCRISPR-TB signal also distinguished individuals with positive vs. negative sputum smear results but not individuals with differing smear positivity grades, despite a trend for increased swab positivity (33 to 96% positive) with increasing smear grade (Fig. 4d). Similarly, swab ActCRISPR-TB signal distinguished TB cases with positive vs. negative Xpert results and very low vs. median and high sputum Xpert grades, with positive results tending to increase with increasing Xpert grade (from 14 to 75% positive) (Fig. 4e); and a similar trend was detected when comparing Xpert Ultra swab and sputum results (Fig. S20). Notably, ActCRISPR-TB swab results detected 33% (31/82) and 14% (3/22) of the TB cases missed by sputum smear and Xpert results.



Subsequent analysis of 52 paired tongue swabs from hospitalized TB cases did not detect ActCRISPR-TB signal differences among the tested swab types (Fig. 4f). However, swabs collected in the morning had higher ActCRISPR-TB signal and positivity rates than those collected at night [median (IQR): 1802 (503, 5128) vs. 1105 (438, 4026); 68% vs. 55% positive] (Fig. 4g), and similar trends were observed for Xpert Ultra results (Fig. S21). Swabs preserved in Tris/EDTA buffer yielded stable signal and positivity when stored at -20°C for 1 week (Fig. 4h). Swab signal but not positivity decreased after 5 days storage

at 4°C , and signal and positivity decreased after 3 and 5 days at room temperature (25°C). Swabs can thus provide useful results after short-term swab storage at conditions encountered in both well-equipped and resource-limited settings.

ActCRISPR-TB LFA diagnostic performance

ActCRISPR-TB assays analyze NA extracts and are read by benchtop instruments, like other reported CRISPR-based TB assays (Table S11)^{11,12,14,23,29–60}, and are thus not practical as point-of-care

Fig. 2 | Study participants. **a** Biobank sputum, BALF, CSF, and stool specimens analyzed to determine the diagnostic performance of ActCRISPR-TB for pulmonary and extrapulmonary TB, and their characteristics. Diagnostic criteria for **(b)** clinician-collected and **(c)** self-collected tongue swab specimens analyzed by Xpert Ultra and benchtop ActCRISPR-TB and point-of-care ActCRISPR-TB LFA. Created in BioRender. Huang, Z. (2025) <https://BioRender.com/9l03cm7>. *TB (Table S5, S7, S10, and S13) and *TBM (Table S9) classifications were assigned post-hoc according to the *China Clinical Treatment Guide for Tuberculosis* and *2019 Chinese Guidelines for the Diagnosis and Treatment of Central Nervous System Tuberculosis*, respectively. [†]HIV-positive adult participants were classified based on clinical

presentation, laboratory findings, and treatment response, as determined by expert panel review (Table S6). [‡]Children were considered MRS-positive (MRS+) if they had sputum, gastric aspirate, or stool specimens that tested positive by Xpert Ultra, or had positive culture or smear results; and were otherwise classified as MRS-negative (MRS-) (Table S8). Abbreviations: BALF bronchoalveolar lavage fluid, CDTB clinical diagnosed TB, CDTBM clinical diagnosed tuberculous meningitis, CSF cerebrospinal fluid, CXR chest X-ray, IGRA interferon gamma release assay, LFA lateral flow assay, NGS Next-generation sequencing, MRS microbiological reference standard, TB tuberculosis, TBM tuberculous meningitis, Xpert GeneXpert MTB/RIF.

assays, which should minimize operator and equipment requirements. We therefore refined the ActCRISPR-TB workflow, employing a simple thermal/mechanical lysis procedure to generate sample lysates that could be directly analyzed by the assay, yielding signal that could be visualized using a LFA (Fig. 5a). This streamlined ActCRISPR-TB LFA workflow employed a 10-min thermal/mechanical lysis step to release *Mtb* DNA, a 45-min ActCRISPR-TB reaction, and a 2-min LFA incubation step, followed by visual or smartphone detection approaches that respectively produced qualitative or semi-quantitative results (Fig. 5b and S22–24). Sample classification results obtained with thermal/mechanical lysates were equivalent to those determined with standard NA extracts despite yielding slightly weaker signal, and significantly reduced workflow complexity, time, and cost (Fig. S25; Table S12).

Sensitivity and specificity results for the optimized ActCRISPR-TB LFA and benchtop ActCRISPR-TB assay were comparable (Fig. 5c, d and S26). Weakly and moderately positive swabs spiked with 10 and 100 target copies/μL did not exhibit signal variability detectable by visual inspection, but smartphone readouts detected 2.3% to 15.6% intra-assay and 9.9% to 14.5% inter-assay coefficients of variation (Fig. 5e). Food residue attenuated signal intensity but not positive signal identification rates in weakly positive spiked swabs samples (Fig. 5f).

ActCRISPR-TB benchtop and LFA results for self-collected tongue swabs detected 17 of 24 TB cases and 0 of 11 non-TB controls (Fig. 5g; Table S13). Notably, three weakly positive ActCRISPR-TB LFA results detected at 45 min were readily detected when read by smartphone (Fig. S27) and had strongly positive visual results when read at 90 min (Fig. S28). Xpert Ultra swab results detected 16 TB cases, including 15 with positive ActCRISPR-TB benchtop/LFA results, with the former and latter assays uniquely detecting one and two additional TB cases and missing six TB cases (Fig. 5e and S29a), despite Xpert Ultra using 40-fold more lysate. Sputum Xpert results detected more true-positives than ActCRISPR-TB LFA swab results, but missed one case identified by ActCRISPR-TB, and both returned false-negative results for two TB cases (Fig. S29b).

Discussion

Streamlined versions of existing CRISPR assays can serve as promising foundations for new molecular diagnostics, particularly those that can be used in remote and resource-limited settings where improved disease screening is critical. Our findings demonstrate that one-pot ActCRISPR-TB assays provide straightforward and sensitive means to diagnose TB, a significant public health challenge that remains underdiagnosed worldwide, often due to test limitations. Traditional microbiologic assays can take weeks to yield useful results, substantially delaying TB diagnosis^{4,61}, while rapid and sensitive molecular TB tests, such as Xpert and Xpert Ultra, require expensive equipment and infrastructure that is often unavailable in high TB burden regions^{61,62}. Streamlined one-pot molecular assays, such as ActCRISPR-TB, that integrate isothermal amplification and CRISPR-mediated target detection without requiring expensive equipment could thus prove useful for sensitive and specific point-of-care screening efforts^{6,63}.

Cas12a can have complex interactions with RPA amplicons in integrated RPA-CRISPR systems to affect the activity of both reactions. The recombinase activity and ssDNA binding proteins of the RPA reaction promote and stabilize dsDNA unwinding to enable primer annealing and strand-displacement polymerase amplification, yielding ssDNA intermediates and dsDNA amplicons that can activate both Cas12a cis- and trans-cleavage activity^{17,22}. Cas12a cleavage of either of these products could thus restrict amplicon accumulation and attenuate RPA and Cas12a activity, as both are regulated by target amplicon abundance^{8,16}, although asymmetric Cas12a activity associated with non-consensus PAMs appears dsDNA-specific since ssDNA-induced Cas12a activation appears to be PAM-independent⁸. PAM sites were first reported as essential for Cas12a activation⁶⁴, but subsequent results have shown that they facilitate DNA unwinding without affecting Cas12a cleavage activity^{17,65}. R-loop-induced changes in RuvC domain conformation have instead been shown to drive Cas12a activation⁶⁶, and support PAM-independent cleavage, so that cleavage efficiency is primarily regulated by stable R-loop formation determined by gRNA binding affinity, Cas12a RNP concentration, and ionic strength⁶⁷. Recent studies have therefore used gRNAs targeting sequences with non-consensus PAMs or engineered gRNAs¹⁹ to attenuate cis-cleavage and improve target detection, although these efforts also often attenuate reporter trans-cleavage and assay sensitivity^{7,8}. Studies have also revealed the independence of Cas12a cis- and trans-cleavage activity^{21,22}, suggesting that selecting gRNA targets that favor trans-cleavage could enhance the sensitivity of one-pot RPA-CRISPR assays. This agrees with our findings that three gRNAs (gRNA-4, -5, and -6) that recognize targets with non-consensus PAMs yielded Cas12a RNP activity profiles biased toward trans-cleavage to enhance their assay kinetics. These findings agree with a recent study reporting Cas12a cis-cleavage was not required for trans-cleavage, and that these activities could be independently altered by variations in non-consensus PAM sequence²³.

Signal production by standard CRISPR assays is proportional to target concentration but can be enhanced by using multiple RNPs that bind distinct sites on a target. We observed that assays using multiple gRNAs sometimes revealed improved kinetics, although the magnitude this effect was less than reported in a previous study using an amplification-free assay⁹. This may be due to the competition between the RPA and Cas12a reactions that could accelerate amplicon depletion when multiple RNPs are used in an integrated RPA-CRISPR reaction, even when the total RNP concentration does not change. Steric hindrance among RNPs that bind adjacent recognition sites, or other competitive effects, could also attenuate signal production, since we used a short target fragment (208 bp) with limited gRNA recognition site separation. Such competitive effects could be mitigated by using larger target sequences and more dispersed gRNA recognition sites to facilitate efficient RNP binding and cleavage.

Sputum has been the preferred sample for pulmonary TB diagnosis, but its poor diagnostic performance in some patient groups can limit its utility and require consideration of alternative respiratory specimens, such as BALF and gastric aspirates²⁵. Non-respiratory specimens required to directly diagnose EPTB also have difficult collection

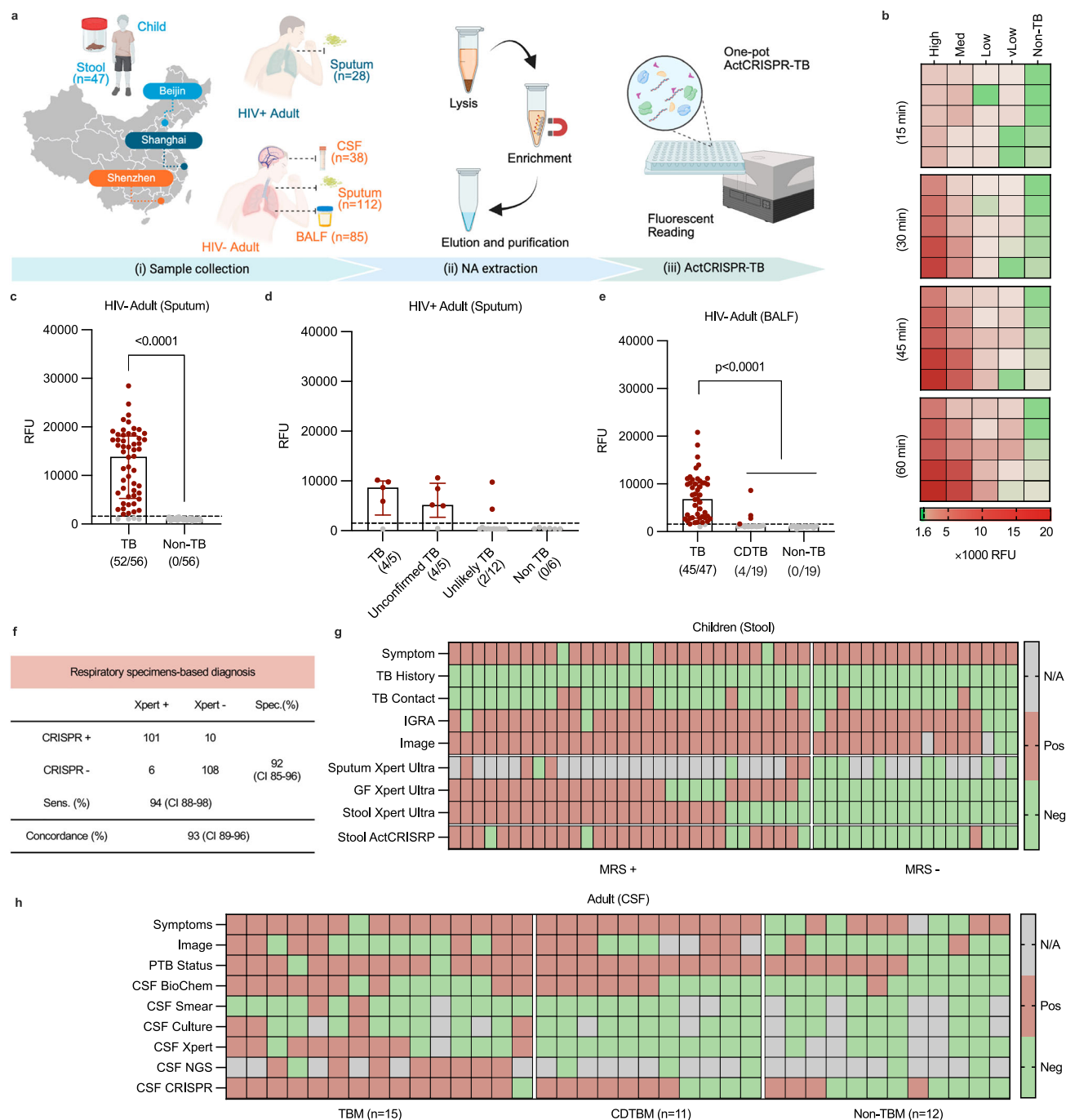


Fig. 3 | ActCRISPR-TB diagnostic performance for pulmonary and extrapulmonary TB. a Schematic of the ActCRISPR-TB workflow for TB diagnosis, indicating the patient enrollment sites, patient populations, and the collected diagnostic specimen types [sputum, bronchoalveolar lavage fluid (BALF), cerebrospinal fluid (CSF), and stool] and magnetic bead-based nucleic acid extraction, and fluorescence-based ActCRISPR-TB readout protocols. The depiction of China in the map omits the South China Sea area. Created in BioRender. Huang, Z. (2025) <https://BioRender.com/di4crxt> **b** Heatmap of ActCRISPR-TB signal detected for sputum specimens with high (Ct < 16), medium (Ct 16–22), low (Ct 22–28), and very low (Ct > 28) GeneXpert MTB/RIF (Xpert) grades at the indicated time points. Arrays indicate signal detected from 25 specimens arranged in columns according to their Xpert grade and analyzed at the indicated successive timepoints. ActCRISPR-TB signal and positivity detected in sputum DNA samples from **c** 112 HIV- adults with TB or non-TB diagnoses, and **d** 28 HIV+ positive adults with TB, unconfirmed TB, unlikely TB, and non-TB diagnoses. **e** ActCRISPR-TB signal and positivity detected for BALF specimens from 85 adults with TB or clinically diagnosed TB (CDTB) or non-TB diagnoses. **f** ActCRISPR-TB vs. Xpert overall diagnostic sensitivity (Sens.) and specificity (Spec.) estimates and 95% confidence intervals for pooled sputum and BALF results. **g** Clinical findings for 47 children judged to have microbiological reference standard (MRS)-positive and negative, including symptoms, TB history and exposure, interferon gamma release assay (IGRA), radiographic image, and Xpert testing results on specimens. **h** Clinical findings for 38 adults with confirmed tuberculous meningitis (TBM), clinically diagnosed TBM (CDTBM), or non-TBM diagnoses, including symptoms, radiographic image and CSF test results, and pulmonary TB (PTB) diagnostic status. Bar graphs in (c–e) depict medians with interquartile ranges, *p* values calculated with two-sided the Mann-Whitney tests, and black dashed lines indicating the positive-signal threshold defined by the non-TB group. Source data are provided as a Source Data file.

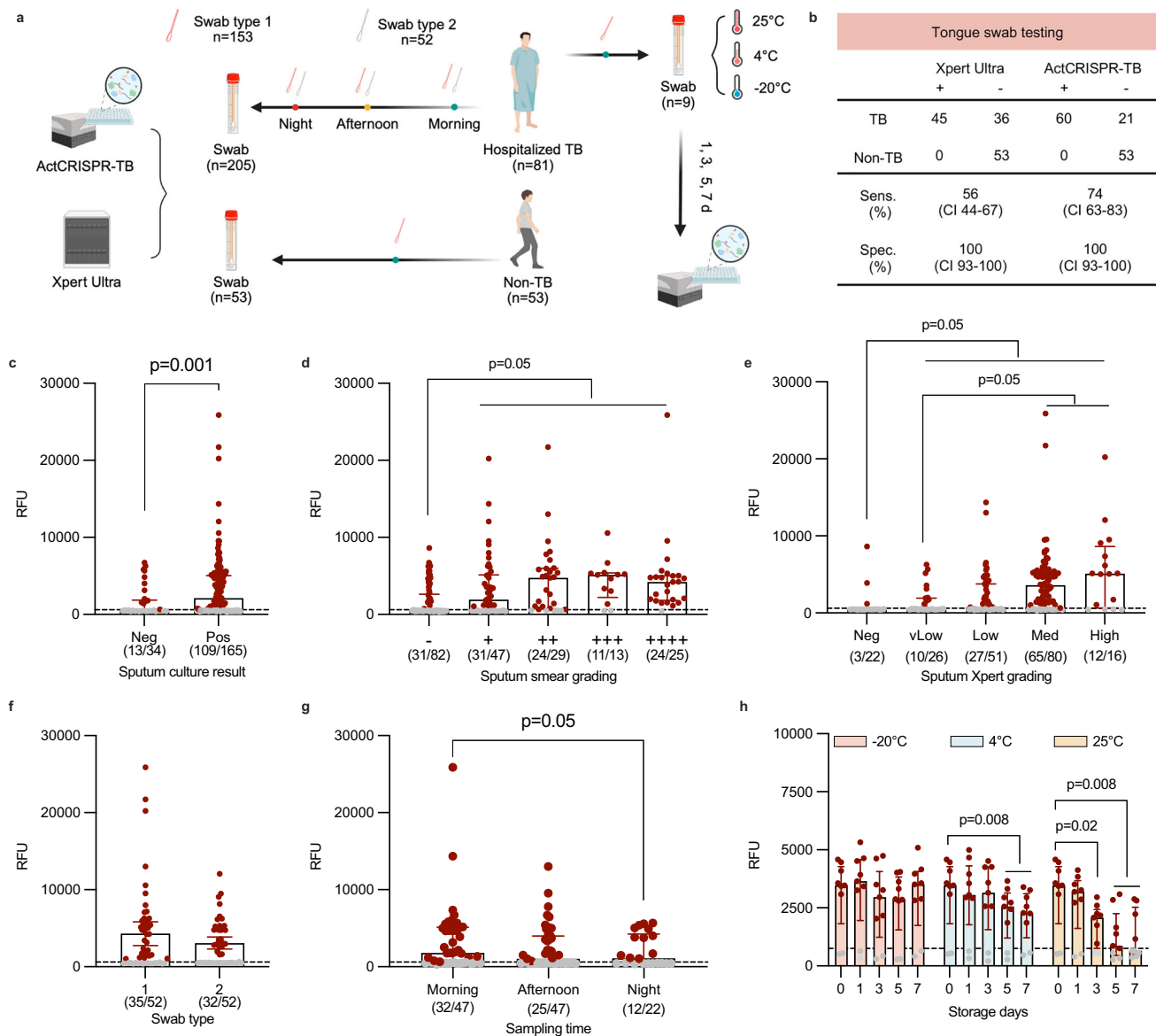


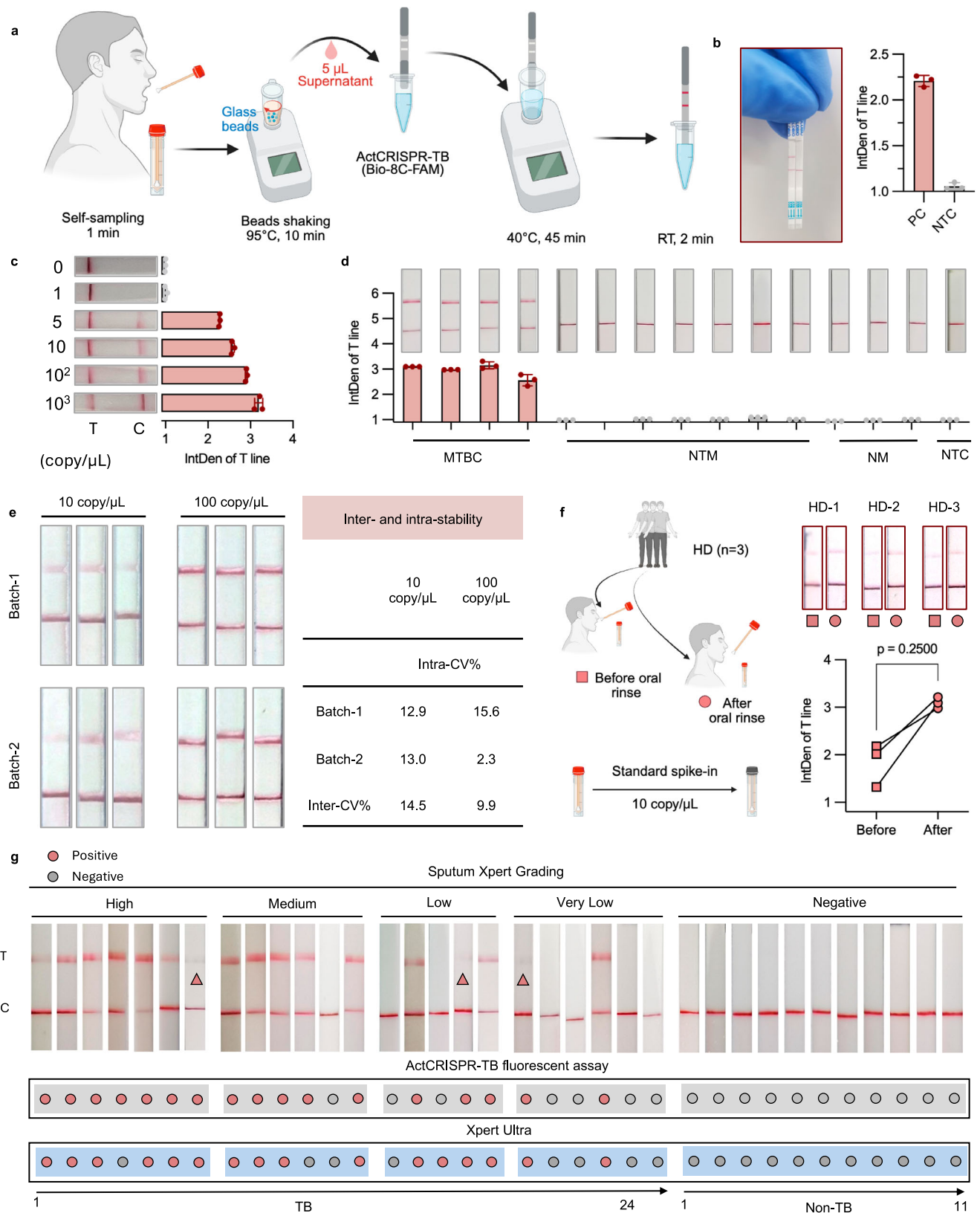
Fig. 4 | ActCRISPR-TB diagnosis of pulmonary TB with tongue swabs. a Study design and workflow for tongue swab collection and preservation. Created in BioRender. Huang, Z. (2025) <https://BioRender.com/14wqty8>. **b** ActCRISPR-TB and Xpert Ultra diagnostic performance with tongue swabs collected from this cohort. Image created with BioRender.com. ActCRISPR-TB signal and positivity for tongue swabs stratified by sputum *c* *Mtb*-culture, **d** smear grade, and **e** Xpert grade results. ActCRISPR-TB signal and positivity for swab specimens collected with **f** different

swab types and **g** at distinct intervals, or after variable length storage at different temperatures. Bar graphs depict median and interquartile ranges, with black dashed lines indicating the positive signal threshold. Statistical significance was evaluated using two-sided Mann-Whitney tests (**c–e, h**), and two-sided Wilcoxon signed-rank test (**f, g**). Abbreviations: Med medium, Neg Negative, Sens sensitivity, Spec specificity, vLow very Low. Source data are provided as a Source Data file.

processes and low positivity rates²⁷, complicating EPTB diagnosis. ActCRISPR-TB CSF results sensitively diagnosed TBM, detecting cases missed by Xpert and other assays, but also detected unexpected false positives for several individuals diagnosed with pulmonary TB. These results could indicate the ability of ActCRISPR-TB to detect early-stage TBM, or represent TBM false positives due to *Mtb* DNA dissemination from another anatomical site via the circulation⁶⁸ or aerosol contamination during liquid handling, underscoring the need for stringent practices when employing sensitive molecular assays. Such false positives are unlikely to arise from deficient assay specificity, however, as this would require both off-target RPA amplification and Cas12a RNP recognition.

Molecular diagnostics tailored for use in remote and resource-limited settings must consider sample collection practicalities and

prioritize specimens that are easily obtained without clinical personnel. Specifications for new TB diagnostics, for example, indicate that they should be affordable, decentralized, and capable of utilizing non-sputum specimens to allow their widespread use for TB screening to narrow the current case detection gap and reduce community TB transmission⁴. Our proof-of-concept ActCRISPR-TB LFA can address all these criteria, as it sensitively and cost-effectively detects *Mtb* DNA from self-collected tongue swabs of TB suspects without requiring expensive and complex equipment. However, we observed that 26% of TB cases with positive sputum results had negative tongue swab results. *Mtb* DNA levels are lower on the tongue than in sputum^{28,69}, and can vary with differences in sample collection, disease burden, infection site distribution, and host activity^{70,71}, which can influence the respiratory material transfer to and depletion from the oral cavity, all



of which can complicate the translation of swab-based diagnostics into clinical practice. Lessons from COVID-19 testing suggest that repeat testing, the use of more homogeneous saliva samples, and other strategies could offer potential solutions².

The incomplete integration of ActCRISPR-TB may constrain its diagnostic utility, and further revision may be required to develop a

sample-in/result-out system that fully integrates sample preparation, detection, and interpretation into a streamlined workflow. Nevertheless, ActCRISPR-TB LFAs favorably compare with reference Xpert and Xpert Ultra as they do not require additional expensive equipment, are faster, and have better or comparable sensitivity at lower cost. The ActCRISPR-TB LFA per test cost should also decrease at scale,

Fig. 5 | ActCRISPR-TB LFA analysis of self-collected tongue swab specimens. **a** Sample collection/processing, ActCRISPR-TB, and LFA readout workflow. Created in BioRender. Huang, Z. (2025) <https://BioRender.com/Osilymt>. **b** ActCRISPR-TB LFA images and results for **b** no-template control (NTC) and positive control (PC) samples, **c** IS6110 DNA concentration standards, and **d** lysates of four *Mtb* complex (MTBC), seven non-tuberculous mycobacteria (NTM), and three non-mycobacterial (NM) species. **e** Inter- and intra-assay coefficients of variation for ActCRISPR-TB LFA results of spiked tongue swab samples (10 and 100 copies/μL) tested with two test strip batches. **f** ActCRISPR-TB LFA images and results for postprandial tongue swabs collected before and after oral rinse from healthy donors (HD, *n* = 3) and then spiked with IS6110 DNA (10 copies/μL). Created in BioRender. Huang, Z. (2025) <https://BioRender.com/execr4a>. **g** ActCRISPR-TB LFA images and ActCRISPR-TB

and Xpert Ultra results for self-collected tongue swabs of 35 adults diagnosed with (*N* = 24) and without (*N* = 11) TB (Table S13). All TB patients were stratified into four categories based on their semi-quantitative sputum Xpert MTB/RIF grades as a proxy for sputum *Mtb* burden: high (Ct < 16), medium (Ct 16–22), low (Ct 22–28), and very low (Ct > 28). Pink triangles denote weakly positive LFA results, and red and gray dots indicate positive and negative ActCRISPR-TB and Xpert Ultra results. Bar graphs represent mean ± SD results calculated from three independent LFA reads, and a *p* value calculated with a two-sided Wilcoxon signed-rank test. IntDen (Integrated Density) indicates the colorimetric intensity of the T-line, as determined by the total pixel intensity detected within this region of the test strip when measured by ImageJ. Source data are provided as a Source Data file Abbreviations: RT room temperature.

as its major expense derives from the small-scale sourcing of its LFA test strips and RPA reagents (Table S12). ActCRISPR-TB LFA temperature stability was not analyzed in this study, but we have previously reported that a similar RPA-CRISPR TB assay retained full activity after 8 weeks storage at 25 °C, the highest analyzed temperature, whereas Xpert assays are reported to retain activity for 6 weeks when stored between 2 and 45 °C⁵⁹. ActCRISPR-TB LFA workflow and diagnostic characteristics also match or exceed those of other reported CRISPR-based one-post TB diagnostics (Table S11).

Several factors influence the interpretation of our results. First, although the TB cohorts analyzed in this study attempt to cover the spectrum of TB disease and include populations and manifestations that are more difficult to diagnose, there were relatively few specimens available for analysis in some of these groups. Future studies will therefore need to validate our findings in larger prospective cohorts to better capture the diversity of these groups. Second, our pilot study performed with tongue swabs obtained from hospitalized TB cases with culture/Xpert-positive sputum results does not address the feasibility of employing this approach in community-based active TB detection efforts that screen primarily asymptomatic populations where affected individuals predominantly have low *Mtb* burden²⁸. Further studies should thus evaluate the utility of this approach in community populations and its potential to identify sub-clinical TB cases. Third, we observed that swab collection and storage protocol differences influenced assay performance, highlighting the need for systematic procedure optimization and standardization prior to clinical translation. At least one study has addressed this issue⁶⁹, but further studies are required to develop standard practices for sample collection. Finally, while previous studies have reported that assays using lyophilized CRISPR reagents exhibit good performance⁷², we did not test the stability of ActCRISPR-TB LFA performance after ambient storage. Future clinical studies will need to validate ActCRISPR-TB LFA performance following storage under conditions representative of those found in at screening sites in regions with high TB burden.

These findings provide preliminary evidence that RPA-CRISPR assays that employ multiple RNPs favoring trans- vs. cis-cleavage activity can enhance assay sensitivity and kinetics. Successful application of this strategy to new molecular diagnostics should permit development of sensitive and streamlined point-of-care assays that should facilitate disease diagnosis and management efforts in regions now underserved by modern diagnostics to improve global health outcomes.

Methods

Ethical statement

Clinical samples and de-identified clinical results, and patient information (self-reported age and gender) analyzed in this study were collected from electronic medical records systems after obtaining written informed consent, using protocols approved by the Ethical Review Boards of the Third People's Hospital of Shenzhen (2023-051

and 2024-005), Huashan Hospital (KY2023-515), Shanghai Public Health Clinical Center (2024-S051-03), and Beijing Children's Hospital (2025-Y-040-D), and was disclosed on the National Health Security Information Platform of China (MR-44-24-014255). The study was registered in the National Health Security Information Platform of China (MR-44-24-014255).

Key supplies

RPA kits were obtained from three commercial suppliers [Jiangsu Qitian Gene Biotechnology (B00000); Amp-Future Biotech (WLB8201KIT); and TwistDx. (TABAS03KIT)]. Cas12a (32108), HOLMES buffer (32005), magnetic bead-based nucleic acid extraction kits (36114-01), and lateral flow strips (31203-02; Lot 24008801 and 24429601) were purchased from Tolo Biotech. Primers, gRNAs, and reporter oligonucleotides (Table S1 and Supplementary Data 1) were synthesized by Sangon Biotech. Nuclease-free water was purchased from ThermoFisher Scientific (4387936) and swab-1 and swab-2 tongue swabs were obtained from Copan Diagnostics (FLOQSwab, SE075S01) and MEIDIKE GENE (FlockingSwab MFS-98000KQ-A). *Mtb* complex, non-tuberculosis mycobacteria, and non-mycobacteria strains (Table S2) were obtained from ATCC or clinical isolates.

Two-step CRISPR-TB assay

A two-step CRISPR-based TB assay using separate RPA preamplification and CRISPR detection steps was performed as described previously¹¹. Lyophilized RPA pellets were dissolved in 29.4 μL RPA buffer, mixed with 2 μL primer solution (10 μM each), 2.5 μL MgCl₂ (280 nM), and 11.1 μL nuclease-free water, then mixed with 5 μL of a nucleic acid sample and incubated at 37 °C for 30 min. A 2 μL aliquot of this reaction was then mixed with 28 μL of CRISPR reaction reagents (3 μL of 10 × HOLMES Buffer, 1 μL of 1 μM gRNA, 1 μL of 1 μM Cas12a, 1.5 μL of 10 μM fluorescent reporter-1, and 21.5 μL of nuclease-free water), and incubated at 37 °C for up to 60 min in a fluorescence plate reader, with CRISPR-generated signal (excited at 485 nm and read at 525 nm) recorded each minute.

ActCRISPR-TB assay

ActCRISPR-TB assays were performed by mixing 17.5 μL of solution A and 2.5 μL of solution B with and 5 μL of sample, incubated at 37 °C for up to 60 min in a fluorescence plate reader, with CRISPR-generated signal (excited at 485 nm and read at 525 nm) recorded each minute. Solution A was prepared by dissolving RPA enzyme powder in 29.4 μL RPA buffer, which was then mixed with 1.25 μL of forward/reverse primer solution (20 μM each), 3 μL MgCl₂ (280 mM), and 1.35 μL nuclease-free water by gentle shaking. Solution B was prepared by mixing 0.1 μL gRNA (10 μM), 0.1 μL Cas12a (10 μM), 1.5 μL of 10 μM reporter-1, and 0.8 μL nuclease-free water. Optimum reaction conditions were determined by systematically adjusting primer, Mg²⁺, RNP, and reporter concentrations, reaction temperature, and the RPA kit used.

ActCRISPR-TB LFA assay

ActCRISPR-TB LFA reactions mixed 17.5 μL of solution A and 2.5 μL of solution B (replacing reporter-1 with 12.5 nM reporter-20) with 5 μL of sample and incubated this reaction mixture at 37 °C for 45 min. An LFA strip was then inserted into the reaction tube, incubated at room temperature for 2 min, and read by visual inspection or quantified using a smartphone, where images of LFA results were captured, cropped to the appropriate region, and converted to 8-bit grayscale using NIH ImageJ software (1.54J, Fig. S18). LFA background was then subtracted (rolling ball radius: 50 pixels), images were inverted, and signal intensity at T-line area was quantified using a fixed rectangular selection box. Each image was captured and analyzed three times to avoid random variations, and the same rectangular selection area encompassing the entire T-line region was consistently applied to all replicates to ensure analytical consistency. The cut-off value for positive signal was defined as the mean of the NTC plus three times its standard deviation. Reporter concentration was optimized to minimize background by directly applying serial dilutions of reporter-2 (100, 50, 25, 12.5, 6.25, 3.13, and 0 nM) to LFA strips, with the optimum reporter concentration defined as the lowest concentration that generated detectable signal at the C-line without producing T-line signal.

To assess intra- and inter-batch coefficients of variations of the LFA strips, two LFA strip batches were used to analyze ActCRISPR-TB LFA results from samples spiked with 10 or 100 IS6110 copies/ μL , with three technical replicates per condition. To assess the effect of food residue, tongue swabs were collected 1 h after lunch from health donors ($n = 3$) before and after oral rinsing, spiked with 10 IS6110 copies/ μL and then analyzed by ActCRISPR-TB LFA.

Characterization of RNP cis-cleavage activity

Cas12a cis-cleavage reactions (30 μL) containing 13.3 μM IS6110 target DNA and 0.5 μM RNP were incubated at 37 °C, and 5 μL aliquots were removed at 30, 45, and 60 min, heat inactivated for 30 s at 60 °C, then analyzed by gel electrophoresis, after which target band intensities were measured using ImageJ. Relative Cas12a cis-cleavage activity was defined as the percent reduction in target band intensity in reactions with vs. without added Cas12a (Fig. S4).

Characterization of RNP trans-cleavage activity

Cas12a trans-cleavage activity induced by different gRNAs was assessed using the Michaelis–Menten equation ($V_0 = V_{\text{max}} [S]/(K_m + [S])$), where V_0 was the rate at which the signal grew linearly during the initial reaction phase, $[S]$ was the reporter concentration, V_{max} was the maximum reaction rate, and K_m was the Michaelis constant²⁰.

Cas12a Trans-cleavage reactions (30 μL) containing 1 nM RNP and sequential concentrations of fluorescent reporter-1 (0, 3.9, 7.8, 15.6, 31.2, 62.5, 125, 250, 500 and 1000 nM) were performed in triplicate at 37 °C and which was initiated by the addition of 13.3 μM IS6110 target DNA. Fluorescent signal was read every 60 s for at least 10 min, and the first 10 min of signal was subjected to linear fitting to calculate V_0 (RFU/s), which was converted to the probe cleavage rate (nM/s) using fluorescence intensity–reporter concentration standard curves (Fig. S5).

Standard curves were generated using CRISPR reactions containing 0 or 100 nM template and sequential reporter concentrations (0, 25, 50, 100, 200, 400, 800, and 1600 nM) and analyzed every 30 s until attaining maximum signal. The background-subtracted un-cleaved (RFU_{ucl}) and cleaved (RFU_{cl}) reporter signal values were respectively calculated for the 0 and 100 nM template reactions, by subtracting their maximum 0 nM reporter reaction signal from all other reactions. Linear fitting of the RFU_{ucl} and RFU_{cl} values of these reactions versus their input reporter concentrations (C_{ucl} and C_{cl}) was then used to derive their slopes (S_{ucl} and S_{cl}) (Fig. S5). The cleavage reporter concentration as a function of time (t) was then derived using

the following equation:

$$C_{\text{cl}}(t) = \frac{F(t) - C_0 S_{\text{ucl}}}{S_{\text{cl}} - S_{\text{ucl}}}$$

Where $F(t)$ represents the fluorescence measured at a specific time, $C_{\text{cl}}(t)$ denotes the concentration of the cleaved probe at that time, and C_0 corresponds to the initial concentration of un-cleaved reporters.

The catalytic rate (K_{cat}) and Michaelis constant (K_m) determined for the reaction rate versus reporter concentration were then fitted to the Michaelis-Menten equation.

Specificity analysis

Supernatants of pathogen cultures (Table S2) were harvested, incubated at 95 °C for 30 min, and sonicated, these homogenates were then centrifuged to remove debris, and their supernatants were stored at –80 °C for subsequent analysis. Specificity of the seven tested gRNAs was evaluated by analyzing 2 μL of these lysates with the two-step CRISPR-TB assay and the optimized ActCRISPR-TB assay.

Clinical sample and information collection

Matching sputum, BALF, stool, and CSF biobank specimens archived after patient diagnosis or treatment were selected using predefined criteria from patients with complete clinical information and clear diagnostic outcomes. Sputum and BALF specimens had Xpert results, stool samples had Xpert Ultra results, and CSF samples had Xpert and/or NGS results, provided they had >1 mL or >0.05 g of sample available for analysis. Equal numbers of patients with positive and negative sputum samples were included in this study, whereas all patients with BALF and CSF specimens were included in our analyses.

Prospective specimens were obtained from 81 adults consecutively enrolled between December 12, 2023 and March 12, 2024 after receiving confirmed TB diagnoses due to their sputum microbiological and/or molecular test results. These patients had not received anti-TB treatment in the past 6 months and received no more than 1 week of anti-TB treatment at specimen collection. Sputum Xpert tests were performed within 3 days before tongue swab collections to provide a reliable reference result. All TB patients had at least one sample collected with two different swab types by trained professionals in the morning (9:00–10:00), afternoon (15:00–16:00), and/or evening (20:00–21:00). Non-TB patients and healthy volunteers were recruited from TB outpatient clinics and laboratory teams between December 12 and December 20, 2023, after undergoing symptom screening, TB history evaluation, chest X-rays, and IGRA testing. TB cases were excluded from this group by their sputum Xpert results, and non-TB patients had only morning tongue swabs collected using swab-1. Self-collected tongue swab specimens were obtained from patients after instruction and tested by Xpert Ultra and ActCRISPR-TB desktop/LFA tests.

Swab specimens were transferred to 1 mL of TE buffer, immediately transported to the testing laboratory, stored at –20 °C overnight, and then tested by Xpert Ultra and ActCRISPR-TB. Nine additional morning swab-1 samples were collected from a subset of TB patients and aliquoted into 50 μL aliquots that were stored at –20 °C, 4 °C, and 25 °C until tested with ActCRISPR-TB at designated time points (0, 1, 3, 5, and 7 days).

Clinical sample preparation

Clinical samples (sputum, BALF, CSF) were mixed with 4% NaOH at a 1:2 ratio, incubated at room temperature for 30 min, centrifuged at 13,800 $\times g$ for 3 min. Precipitates were resuspended in 800 μL of supernatant and mixed with 20 μL of magnetic beads and vortexed at 1000 rpm for 3 min. Magnetic beads were collected via magnetic separation, sequentially washed with 200 μL Wash Buffer 1 and Wash Buffer 2 then incubated at room temperature for 5 min to air dry, and

vortexed at 5000 rpm for 2 min in the presence of 50 μ L of elution buffer. Magnetic beads were then collected via magnetic separation and the nucleic acid supernatants were then collected and stored at -80°C until use.

Small (0.6–0.8 g) stool samples were mixed with 1 mL of sterile water containing ~ 100 mg of glass beads, vigorously vortexed for ≥ 30 s, allowed to settle for 10 min, and then 1 mL of supernatant was collected, avoiding solid debris, and processed for nucleic acid extraction as previously described for sputum samples.

Swab samples for ActCRISPR-TB and ActCRISPR-TB LFA were prepared by adding ~ 100 mg of glass beads (Sigma-Aldrich inc., G8772) to 200 μ L of swab preservation solution, and then vortex mixing these samples at 95°C for 10 min at 2000 rpm on a heated vortex mixer. Samples were then incubated at room temperature for 1 min, quick spun to pellet the glass beads, and 5 μ L of the collected supernatant added to an ActCRISPR-TB assay.

Structural representations of LbCas12a/gRNA/dsDNA complexes

Three-dimensional structures of LbCas12a proteins complexed with distinct gRNAs and their double-stranded DNA (dsDNA) targets were predicted with the AlphaFold 3 protein structure prediction web platform (<https://alphafoldserver.com>)⁷³. Based on the published complex structure⁷⁴, two magnesium ions were incorporated into each computational model as catalytic cofactors to preserve enzymatic activity during RNP structure prediction.

Statistics and reproducibility

Signals from nonclinical samples (IS6110 standards and pathogen DNA extracts) were normalized to the maximum detected signal in the same experiment. The positive signal threshold was defined as the mean signal of the non-template control group plus 3 times its standard deviation. Clinical validation was conducted with all available samples without performing an a priori sample size estimate. Laboratory personnel responsible for sample testing were blinded to the clinical classification data until the analysis stage. No data were excluded from the analysis. Participant characteristics were summarized using medians, IQRs, and proportions. Significant signal differences between groups were determined using Mann-Whitney test or Wilcoxon signed-test ($\alpha = 0.05$). The 95% confidence intervals of sensitivity and specificity estimates were calculated assuming a binomial distribution. Gender-based analyses were not performed since gender was not found to influence diagnostic performance. Quantitative analysis of test strip signals was performed using NIH ImageJ software (1.54J) and all statistical analyses and data visualization were performed using GraphPad Prism software (10.1.1).

Reporting summary

Further information on research design is available in the Nature Portfolio Reporting Summary linked to this article.

Data availability

All data generated in this study are provided in the Supplementary Information and Source Data within this paper. The crystal structure used in this work can be found under PDB ID 5XUU. Source data are provided with this paper.

References

- Fleming, K. A. et al. The Lancet Commission on diagnostics: transforming access to diagnostics. *Lancet* **398**, 1997–2050 (2021).
- Yerlikaya, S. et al. Blazing the trail for innovative tuberculosis diagnostics. *Infection* **52**, 29–42 (2024).
- WHO. *Global Tuberculosis Report 2024* (WHO, 2024).
- Pai, M., Dewan, P. K. & Swaminathan, S. Transforming tuberculosis diagnosis. *Nat. Microbiol.* **8**, 756–759 (2023).
- Abou Jaoude, G. J. et al. National tuberculosis spending efficiency and its associated factors in 121 low-income and middle-income countries, 2010–19: a data envelopment and stochastic frontier analysis. *Lancet Glob. Health* **10**, e649–e660 (2022).
- Huang, Z., Zhang, G., Lyon, C. J., Hu, T. Y. & Lu, S. Outlook for CRISPR-based tuberculosis assays now in their infancy. *Front. Immunol.* **14**, 1172035 (2023).
- Gootenberg, J. et al. Nucleic acid detection with CRISPR-Cas13a/C2c2. *Science* **356**, 438–442 (2017).
- Li, S.-Y. et al. CRISPR-Cas12a has both cis- and trans-cleavage activities on single-stranded DNA. *Cell Res.* **28**, 491–493 (2018).
- Fozouni, P. et al. Amplification-free detection of SARS-CoV-2 with CRISPR-Cas13a and mobile phone microscopy. *Cell* **184**, 323–333.e329 (2021).
- Huang, Z., Lyon, C. J., Wang, J., Lu, S. & Hu, T. Y. CRISPR assays for disease diagnosis: progress to and barriers remaining for clinical applications. *Adv. Sci.* **10**, 2301697 (2023).
- Huang, Z. et al. CRISPR detection of circulating cell-free *Mycobacterium tuberculosis* DNA in adults and children, including children with HIV: a molecular diagnostics study. *Lancet Microbe* **3**, e482–e492 (2022).
- Thakku, S. G. et al. Genome-wide tiled detection of circulating *Mycobacterium tuberculosis* cell-free DNA using Cas13. *Nat. Commun.* **14**, 1803 (2023).
- Liu, T. Y. et al. Accelerated RNA detection using tandem CRISPR nucleases. *Nat. Chem. Biol.* **17**, 982–988 (2021).
- Ai, J. W. et al. CRISPR-based rapid and ultra-sensitive diagnostic test for *Mycobacterium tuberculosis*. *Emerg. Microbes Infect.* **8**, 1361–1369 (2019).
- Joung, J. et al. Detection of SARS-CoV-2 with SHERLOCK one-pot testing. *N. Engl. J. Med.* **383**, 1492–1494 (2020).
- Lu, S. et al. Fast and sensitive detection of SARS-CoV-2 RNA using suboptimal protospacer adjacent motifs for Cas12a. *Nat. Biomed. Eng.* **6**, 286–297 (2022).
- Ding, X. et al. Ultrasensitive and visual detection of SARS-CoV-2 using all-in-one dual CRISPR-Cas12a assay. *Nat. Commun.* **11**, 4711 (2020).
- Gleditsch, D. et al. PAM identification by CRISPR-Cas effector complexes: diversified mechanisms and structures. *RNA Biol.* **16**, 504–517 (2019).
- Zeng, Q. et al. Rapid and sensitive Cas12a-based one-step nucleic acid detection with ssDNA-modified crRNA. *Anal. Chim. Acta* **1276**, 341622 (2023).
- Ramachandran, A. & Santiago, J. G. CRISPR enzyme kinetics for molecular diagnostics. *Anal. Chem.* **93**, 7456–7464 (2021).
- Chen Janice, S. et al. CRISPR-Cas12a target binding unleashes indiscriminate single-stranded DNase activity. *Science* **360**, 436–439 (2018).
- Nalefski, E. A. et al. Determinants of CRISPR Cas12a nuclease activation by DNA and RNA targets. *Nucleic Acids Res.* **52**, 4502–4522 (2024).
- Xiao, G. et al. Trans-cleavage activity of Cas12a effectors can be unleashed by both double-stranded DNA and single-stranded RNA targeting in absence of PAM. *Int. J. Biol. Macromol.* **309**, 142992 (2025).
- Huerga, H. et al. Novel FujiLAM assay to detect tuberculosis in HIV-positive ambulatory patients in four African countries: a diagnostic accuracy study. *Lancet Glob. Health* **11**, e126–e135 (2023).
- Xu, P. et al. The incremental value of bronchoalveolar lavage for the diagnosis of pulmonary tuberculosis in a high-burden urban setting. *J. Infect.* **79**, 24–29 (2019).
- WHO. *WHO Consolidated Guidelines on Tuberculosis. Module 3: Diagnosis–Rapid Diagnostics for Tuberculosis Detection* (WHO, 2024).

27. Lee, J. Y. Diagnosis and treatment of extrapulmonary tuberculosis. *Tuberc. Respir. Dis.* **78**, 47–55 (2015).
28. Burke, R. M. et al. Community-based active case-finding interventions for tuberculosis: a systematic review. *Lancet Public Health* **6**, e283–e299 (2021).
29. Zhang, Y. et al. Paired design of dCas9 as a systematic platform for the detection of featured nucleic acid sequences in pathogenic strains. *ACS Synth. Biol.* **6**, 211–216 (2017).
30. Xiao, G. H. et al. Cas12a/guide RNA-based platform for rapid and accurate identification of major *Mycobacterium* species. *J. Clin. Microbiol.* **58**, e01368–01319 (2020).
31. Xu, H. et al. An isothermal method for sensitive detection of *Mycobacterium tuberculosis* complex using clustered regularly interspaced short palindromic repeats/Cas12a Cis and trans cleavage. *J. Mol. Diagn.* **22**, 1020–1029 (2020).
32. Li, H. et al. High concentration of Cas12a effector tolerates more mismatches on ssDNA. *FASEB J.* **35**, e21153 (2021).
33. Liu, P. et al. A Recombinase polymerase amplification-coupled Cas12a Mutant-based module for efficient detection of streptomycin-resistant mutations in *Mycobacterium tuberculosis*. *Front. Microbiol.* **12**, 796916 (2021).
34. Sam, I. K. et al. TB-QUICK: CRISPR-Cas12b-assisted rapid and sensitive detection of *Mycobacterium tuberculosis*. *J. Infect.* **83**, 54–60 (2021).
35. Wang, Y. et al. LAMP-CRISPR-Cas12-based diagnostic platform for detection of *Mycobacterium tuberculosis* complex using real-time fluorescence or lateral flow test. *Microchim. Acta* **188**, 347 (2021).
36. Bai, X. et al. A highly sensitive and specific detection method for *Mycobacterium tuberculosis* Fluoroquinolone resistance mutations utilizing the CRISPR-Cas13a system. *Front. Microbiol.* **13**, 847373 (2022).
37. Huang, J., Liang, Z., Liu, Y., Zhou, J. D. & He, F. J. Development of an MSPQC nucleic acid sensor based on CRISPR/Cas9 for the detection of *Mycobacterium tuberculosis*. *Anal. Chem.* **94**, 11409–11415 (2022).
38. Augustin, L. & Agarwal, N. Designing a Cas9/gRNA-assisted quantitative Real-Time PCR (CARP) assay for identification of point mutations leading to rifampicin resistance in the human pathogen *Mycobacterium tuberculosis*. *Gene* **857**, 147173 (2023).
39. Cao, G. et al. Completely free from PAM limitations: asymmetric RPA with CRISPR/Cas12a for nucleic acid assays. *ACS Sens.* **8**, 4655–4663 (2023).
40. Cheng, M. et al. Chain hybridization-based CRISPR-lateral flow assay enables accurate gene visual detection. *Anal. Chim. Acta* **1270**, 341437 (2023).
41. Xiao, J. et al. Development and preliminary assessment of a CRISPR-Cas12a-based multiplex detection of *Mycobacterium tuberculosis* complex. *Bioeng. Biotechnol.* **11**, 1233353 (2023).
42. Zhang, X. et al. A new method for the detection of *Mycobacterium tuberculosis* based on the CRISPR/Cas system. *BMC Infect. Dis.* **23**, 680 (2023).
43. Zhou, M. et al. The construction of CRISPR/Cas9-mediated FRET 16S rDNA sensor for detection of *Mycobacterium tuberculosis*. *Analyst* **148**, 2308–2315 (2023).
44. Chen, M. et al. Toehold-containing three-way junction-initiated multiple exponential amplification and CRISPR/Cas14a assistant magnetic separation enhanced visual detection of *Mycobacterium Tuberculosis*. *ACS Sens.* **9**, 62–72 (2024).
45. Gan, T., Yu, J., Deng, Z. & He, J. ERA-CRISPR/Cas12a system: a rapid, highly sensitive and specific assay for *Mycobacterium tuberculosis*. *Front. Cell. Infect. Microbiol.* **14**, 1454076 (2024).
46. Li, Q. et al. Rapid and highly sensitive detection of *Mycobacterium tuberculosis* utilizing the recombinase aided amplification-based CRISPR-Cas13a system. *Microorganisms* **12**, 1507 (2024).
47. Peng, L. et al. Rapid detection of *Mycobacterium tuberculosis* in sputum using CRISPR-Cas12b combined with cross-priming amplification in a single reaction. *J. Clin. Microbiol.* **62**, e0092323 (2024).
48. Peng, L., Fang, T., Dai, L. & Cai, L. Diagnostic value of cross-priming amplification combined with crispr-cas12b in detecting cell-free dna in tuberculous pleural effusion. *Open Forum Infect. Dis.* **11**, ofae674 (2024).
49. Qiao, Y. et al. Raman-enhanced sensor based on CRISPR-SERS technology for the rapid and hypersensitive detection of *Mycobacterium tuberculosis*. *Anal. Bioanal. Chem.* **416**, 6551–6562 (2024).
50. Qiao, Y. et al. A chemiluminescent sensor based on CRISPR-HCR technology for the hypersensitive detection of *Mycobacterium tuberculosis*. *Anal. Methods* **16**, 7927–7939 (2024).
51. Sun, Y. et al. Point-of-care testing of rpoB in *Mycobacterium tuberculosis* using multiply-primed-RCA coupled with CRISPR/Cas12a. *Heliyon* **10**, e37640 (2024).
52. Taufiq, S., Nagata, M., Abbas, S. R. & Sode, K. An electrochemical biosensor for the detection of tuberculosis specific DNA with CRISPR-Cas12a and redox-probe modified oligonucleotide. *Heliyon* **10**, e40754 (2024).
53. Wu, K., Wu, Z. & Li, X. Clinical diagnostic value of CRISPR-Cas13a-based molecular technology for tuberculosis. *Ir. J. Med. Sci.* **193**, 2889–2895 (2024).
54. Wu, Y. et al. A multi-AS-PCR-coupled CRISPR/Cas12a assay for the detection of ten single-base mutations. *Anal. Chim. Acta* **1320**, 343027 (2024).
55. Bell, A. G. et al. A streamlined CRISPR-based test for tuberculosis detection directly from sputum. *Sci. Adv.* **11**, eadx2067 (2025).
56. Modi, N. H. et al. Simplified co-extraction of total nucleic acids from respiratory samples for detection of *Mycobacterium tuberculosis* and SARS-CoV-2 optimized for compatibility across diagnostic platforms. *medRxiv*. <https://doi.org/10.1101/2025.02.27.25322880> (2025).
57. Wang, W. et al. Amplification-free detection of *Mycobacterium tuberculosis* using CRISPR-Cas12a and graphene field-effect transistors. *Nanoscale* **17**, 4603–4609 (2025).
58. Xiao, G. et al. Direct detection from sputum for drug-resistant *Mycobacterium tuberculosis* using a CRISPR-Cas14a-based approach. *BMC Microbiol.* **25**, 188 (2025).
59. Youngquist, B. M. et al. Rapid tuberculosis diagnosis from respiratory or blood samples by a low cost, portable lab-in-tube assay. *Sci. Transl. Med.* **17**, eadp6411 (2025).
60. Zhang, L. et al. Dual-mode sensing of *Mycobacterium tuberculosis* with DNA-functionalized gold nanoparticles and asymmetric RPA-triggered PAM-free CRISPR system. *Sens. Actuators B Chem.* **424**, 136920 (2025).
61. Walzl, G. et al. Tuberculosis: advances and challenges in development of new diagnostics and biomarkers. *Lancet Infect. Dis.* **18**, e199–e210 (2018).
62. WHO. WHO Standard: Universal Access to Rapid Tuberculosis Diagnostics (WHO, 2023).
63. Huang, Z., Lyon, C. J. & Hu, T. Y. CRISPR-based assays for low-resource settings. *Nat. Rev. Bioeng.* **1**, 230–231 (2023).
64. Swarts, D. C. & Jinek, M. Mechanistic insights into the cis- and trans-acting DNase activities of Cas12a. *Mol. Cell* **73**, 589–600.e584 (2019).
65. Jeon, Y. et al. Direct observation of DNA target searching and cleavage by CRISPR-Cas12a. *Nat. Commun.* **9**, 2777 (2018).
66. Strohkendl, I. et al. Cas12a domain flexibility guides R-loop formation and forces RuvC resetting. *Mol. Cell* **84**, 2717–2731.e2716 (2024).

67. Aris, K. D. P. et al. Dynamic basis of supercoiling-dependent DNA interrogation by Cas12a via R-loop intermediates. *Nat. Commun.* **16**, 2939 (2025).
68. Li, X. et al. Rapid diagnosis of tuberculosis meningitis by detecting *Mycobacterium tuberculosis* Cell-Free DNA in cerebrospinal fluid. *Am. J. Clin. Pathol.* **153**, 126–130 (2019).
69. Steadman, A. et al. New manual quantitative polymerase chain reaction assay validated on tongue swabs collected and processed in uganda shows sensitivity that rivals sputum-based molecular tuberculosis diagnostics. *Clin. Infect. Dis.* **78**, 1313–1320 (2024).
70. Theron, G. et al. Bacterial and host determinants of cough aerosol culture positivity in patients with drug-resistant versus drug-susceptible tuberculosis. *Nat. Med.* **26**, 1435–1443 (2020).
71. Church, E. C. et al. Oral swabs with a rapid molecular diagnostic test for pulmonary tuberculosis in adults and children: a systematic review. *Lancet Glob. Health* **12**, e45–e54 (2024).
72. Nguyen, L. T., Rananaware, S. R., Pizzano, B. L. M., Stone, B. T. & Jain, P. K. Clinical validation of engineered CRISPR/Cas12a for rapid SARS-CoV-2 detection. *Commun. Med.* **2**, 7 (2022).
73. Abramson, J. et al. Accurate structure prediction of biomolecular interactions with AlphaFold 3. *Nature* **630**, 493–500 (2024).
74. Yamano, T. et al. Structural basis for the canonical and non-canonical PAM recognition by CRISPR-Cpf1. *Mol. Cell* **67**, 633–645.e633 (2017).

Acknowledgements

The work was supported by National Natural and Science Foundation of China (82302614 to Z.H.), Shenzhen Fund for Guangdong Provincial High-level Clinical Key Specialties (No. SZGSP010 to S.H.L.), the Medical Scientific Research Foundation of Guangdong Province (A2023170 to Z.H.), the Guangdong Basic and Applied Basic Research Foundation (2025A1515011871 to Z.H.), and the Shenzhen High-level Hospital Construction Fund (23264G1001 to Y.Z.) The researcher efforts of B.N., C.J.L., and T.H. were partially supported by funding provided by Eunice Kennedy Shriver National Institute of Child Health and Human Development (R01HD090927 and R01HD103511 to T.H.), National Institute of Allergy and Infectious Diseases (R01AI144168, R01AI175618, R01AI173021, R01AI174964, R01AI177986, R01AI179714 and R21AI169582-01A1 to T.H.), and U.S. Department of Defense (W81XWH1910026 to T.H.). T.H. also acknowledges the generous support of the Weatherhead Presidential Endowment fund.

Author contributions

Z.H., T.H., and S.H.L. conceived and designed the study. Z.H., Z.S., Y.Z., D.L., H.H., and P.X. contributed to data analysis and interpretation. J.F.Z., X.H.L., M.T.F., Z.Y.W., Y.L.C., L.F., J.C., M.G., L.S., and S.H.L. contributed to clinical information and sample collection and analysis. Z.H. drafted

the manuscript. Z.S., B.N., C.J.L., X.Y.F., T.H., and S.H.L. provided critical revision. Z.H. and S.H.L. have accessed and verified the data, all authors approved the final manuscript, and S.H.L. and T.H. were responsible for the decision to submit the manuscript.

Competing interests

Z.H., Z.S., P.X., and S.H.L. have submitted a patent application to China National Intellectual Property Administration pertaining to the one-pot CRISPR-based TB diagnosis (application number CN202410210237.6). The remaining authors declare no competing interests.

Additional information

Supplementary information The online version contains supplementary material available at <https://doi.org/10.1038/s41467-025-63094-x>.

Correspondence and requests for materials should be addressed to Zhen Huang, Shuihua Lu or Tony Hu.

Peer review information *Nature Communications* thanks Chase Beisel, Maryline Bonnet, and Qingshan Wei, who co-reviewed with Aditi Dey Poonam, for their contribution to the peer review of this work. A peer review file is available.

Reprints and permissions information is available at <http://www.nature.com/reprints>

Publisher's note Springer Nature remains neutral with regard to jurisdictional claims in published maps and institutional affiliations.

Open Access This article is licensed under a Creative Commons Attribution-NonCommercial-NoDerivatives 4.0 International License, which permits any non-commercial use, sharing, distribution and reproduction in any medium or format, as long as you give appropriate credit to the original author(s) and the source, provide a link to the Creative Commons licence, and indicate if you modified the licensed material. You do not have permission under this licence to share adapted material derived from this article or parts of it. The images or other third party material in this article are included in the article's Creative Commons licence, unless indicated otherwise in a credit line to the material. If material is not included in the article's Creative Commons licence and your intended use is not permitted by statutory regulation or exceeds the permitted use, you will need to obtain permission directly from the copyright holder. To view a copy of this licence, visit <http://creativecommons.org/licenses/by-nc-nd/4.0/>.

© The Author(s) 2025